ISSN 0031-918X, The Physics of Metals and Metallography, 2013, Vol. 114, No. 6, pp. 503–513. © Pleiades Publishing, Ltd., 2013.
Original Russian Text © M.V. Ivchenko, V.G. Pushin, A.N. Uksusnikov, N. Wanderka, N.I. Kourov, 2013, published in Fizika Metallov i Metallovedenie, 2013, Vol. 114, No. 6, pp. 549–560.

STRUCTURE, PHASE TRANSFORMATIONS, AND DIFFUSION

Specific Features of Cast High-Entropy AlCrFeCoNiCu Alloys Produced by Ultrarapid Quenching from the Melt

M. V. Ivchenko[a], V. G. Pushin[a, b], A. N. Uksusnikov[a], N. Wanderka[c], and N. I. Kourov[a]

[a] *Institute of Metal Physics, Ural Branch, Russian Academy of Sciences, ul. S. Kovalevskoi 18, Ekaterinburg, 620990 Russia*
[b] *The First President of Russia B. N. Yeltsin Ural Federal University (UrFU), ul. Mira 19, Ekaterinburg, 620002 Russia*
[c] *Helmholtz-Zentrum Berlin for Materials and Energy, Hahn-Meitner-Platz 1, Berlin, 14109 Germany*
e-mail: MVIvchenko@yandex.ru

Received August 30, 2012

Abstract—Results of studying structural and phase transformations that occur in the cast high-entropy equiatomic AlCrFeCoNiCu alloy after ultrarapid quenching from the melt in an inert atmosphere (RQM) and various isothermal treatments are presented for the first time. The investigations have been performed using analytical, transmission and scanning electron microscopy, energy dispersive X-ray spectroscopy, and X-ray diffraction structure and phase analyses, as well as measurements of the nanohardness, microhardness, and elastic moduli. It has been found that an ultrafine-grained structure is formed in this alloy during RQM. Already during quenching and, especially, during subsequent annealing, the alloy undergoes decomposition, which is accompanied by the precipitation in the bcc (*B*2) matrix of some nanosized phases, predominantly of equiaxed morphology, both atomically ordered (*B*2) and disordered (*A*2), with various chemical compositions. All nanophases are multicomponent solid solutions and are enriched in a few elements, which leads to a pronounced nanomodulation of the elemental and phase compositions over the alloy bulk, identified, in particular, from the presence of satellites in the vicinity of some reflections in selected-area electron diffraction patterns.

Keywords: high-entropy equiatomic alloy, ultrarapid quenching, entropy of mixing, spinodal decomposition, structural and phase transformations, nanophases, chemical composition

DOI: 10.1134/S0031918X13060057

INTRODUCTION

Despite the fairly long period of the evolution of materials science as one of the most significant directions of practical and, then, research activities of people, the majority of developed and, in particular, employed inorganic materials are based on one or, more rarely, two or three metals. Among these metals, only twenty or thirty have found wide application, including iron, aluminum, copper, nickel, titanium, tin, lead, zinc, magnesium, niobium, zirconium, and beryllium, as well as precious, refractory, radioactive, and some other metals [1–7]. In the last century, increasing industrial demands for various structural and functional metallic materials have stimulated the advent of new technologies and the development of high-alloy steels and alloys on their basis. The range of alloying elements gradually widens and their fraction in the total mass of materials increases. For example, some grades of steels and alloys, in particular, stainless, high-temperature, and high-strength steels and allows, already contain four or five alloying elements in concentrations of up to 30–40 wt %; high-strength aluminum alloys contain three or four alloying elements in concentrations of up to 10–15 wt %; brasses and bronzes contain alloying elements in concentrations of up to 40 and 15 wt %, respectively [1–9].

On the contrary, in intermetallic compounds, which make up a broad class of atomically ordered compounds of metallic elements, only two or three base elements are used, but their concentrations are higher, e.g., 25–75% in the compounds of A_3B type, and up to 50% in the compounds, such as AB or A_2BC. The intermetallic compounds can be ordered according to various types ($A15$, $B2$, $C15$, $D0_3$, $L1_0$, $L1_2$, $L2_1$, etc.) and sometimes do not possess good structural characteristics and workability, but demonstrate unique functional properties, such as superconductive (Nb_3Sn, V_3Ga), magnetic (compounds of Fe, Ni, and Co), heat-resistance (NiAl, CoAl, CoNiAl), and high-strength (Ni_3Al, Ti_3Al, TiAl) ones. They can also possess shape memory controlled by thermal, deformation, or magnetic effects (TiNi, Ni_2MnGa, etc.) [6–13].

The next important stage of research, which was aimed primarily at improving structural, functional, and processing characteristics of alloys and intermetallic compounds, was related to micro- and macroalloying (by three, four, and five elements), as well as to the development of novel advanced strengthening and

plasticizing methods that involved both the synthesis and the subsequent treatment of poly- and single crystals, as well as the modification and hierarchization of their micro- and submicrocrystalline structures [4–13].

As early as the beginning of the 21st century, the first works appeared on the development and complex study of new so-called high-entropy polymetallic alloys with up to five or six basic components, each in a high concentration (5–35%) [14]. In particular, AlCoCrCuFeNi, CoCrCuFeNiTi, and CuNiAlCoCrFeSi are among these alloys [14–19]. In addition to characteristics typical of metal alloys, they demonstrate unique and unusual properties inherent in, e.g., metal ceramics, including high hardness and resistance to softening at elevated temperatures, a positive thermal strengthening coefficient, high strength characteristics at elevated temperatures, good corrosion resistance, etc. [14–19].

In our previous work [19], we studied the microstructure and the phase and chemical compositions of the multicomponent equiatomic alloy AlCrFeCoNiCu in the initial as-cast state. It is known that, in the alloys of this system, bcc and fcc phases are formed with a dendrite microstructure, the morphology and phase composition of which depend on the chemical composition of an alloy, in particular, on the aluminum concentration [14–16]. In the as-cast equiatomic alloy, lamellar and globular modulated bcc and fcc phases with atomically ordered ($B2$, $L1_2$) and disordered ($A2$) structures were found to form as a result of decomposition in the dendritic matrix; conversely, in the interdendritic spaces, a two-phase mixture of ordered fcc ($L1_2$) phases enriched in copper to various degrees is formed. In this work, the high-entropy alloy of the same nominal composition (AlCrFeCoNiCu) produced by ultrarapid quenching from the melt was comprehensively studied for the first time using primarily modern analytical methods of transmission and scanning electron microscopy.

EXPERIMENTAL

An ingot of high-entropy equiatomic AlCrFeCoNiCu alloy 20 mm in diameter was melted in purified argon; the six alloy components all had a purity of 99.999%. To improve the chemical homogeneity of the alloy, the original ingot was remelted five times, then homogenized in a vacuum furnace for a long time and cooled at a rate of 10 K/s. The alloy was subsequently subjected to RQM, in an inert atmosphere, at a cooling rate of 10^6 K/s using splat quenching. The splat quenching of high-speed melt droplets yields a cooling rate (V_q) of 10^6–10^7 K/s when the droplets collide with a cooling surface, a copper target in our case. We used an explosive charge that ensured a velocity of the drop cloud of up to 300 m/s when the average drop size was from 1 to 13 μm. This method makes it possible to produce a lamellar or flaky specimens with a characteristic diameter of no more than a few centimeters with different thicknesses. Lamellae 40 μm thick were selected for this study.

The alloy was studied in the original RQM state, as well as after annealing at 550 and 600°C. The specimen structure was examined by analytical electron microscopy, namely, transmission electron microscopy (TEM) and scanning electron microscopy (SEM), as well as X-ray diffraction structural and phase analysis (XRD). The electron-microscopic investigations were carried out using Philips CM30 Supertwin (at an accelerating voltage of 300 kV) and Quanta 200-Pegasus (at an accelerating voltage of 30 kV) microscopes. Local chemical analysis was performed using EDAX X-ray energy dispersive spectrometers with which these microscopes were equipped. The electron beam was ~10 nm in diameter in TEM examinations and ~400 nm in SEM examinations. The XRD studies were carried out using Bruker AXS D8 and DRON 3M X-ray diffractometers, by the θ/2θ method in Cu $K\alpha$ monochromatized radiation using mechanically and electrolytically polished specimens. The hardness was measured by a standard microhardness tester. The hardness, elasticity modulus, and creep resistance during nanoindentation were determined on a Fischer Picadentor HM500 instrument equipped with a tetrahedral diamond pyramid with an interfacial angle of 136° under a load of up to 300 mN applied for 20 s. The electrical resistance was measured in the range from room temperature to 650°C at a heating/cooling rates of ~2 K/min using a thin specimen.

RESULTS

The results of X-ray diffraction analysis of the as-cast AlCrFeCoNiCu alloy have shown that the alloy is in a multiphase structural state and contains bcc and fcc phases. Based on the identification of the most intense Bragg reflections, a bcc phase with the lattice parameter $a_{bcc} = 0.288 \pm 0.005$ nm was assumed to be the base matrix phase. In addition, noticeably weaker and broadened reflections from two fcc phases with lattice parameters $a_{fcc1} = 0.362 \pm 0.005$ nm and $a_{fcc2} = 0.359 \pm 0.005$ nm in the form of closely spaced asymmetric doublets were observed. The reflections from the second fcc phase were somewhat stronger. By and large, these results agree with similar data published earlier [14–16, 18]. According to the XRD data, in the RQM alloy produced by splat quenching there is present a single bcc phase exhibiting broadened fundamental and weak superlattice reflections ($a_{bcc} = 0.288 \pm 0.005$ nm).

Figure 1 shows the secondary-electron SEM images of typical structures of the alloy. Figure 1a displays the microstructure of the original RQM alloy, and Figs. 1b and 1c show the microstructure of the alloy annealed at 550°C for 5 h and at 600°C for 2 h, respectively. It follows from the analysis of these figures that ultra-fine grains (UFGs) and, predominantly, submicrocrystalline (SMC) grains less than

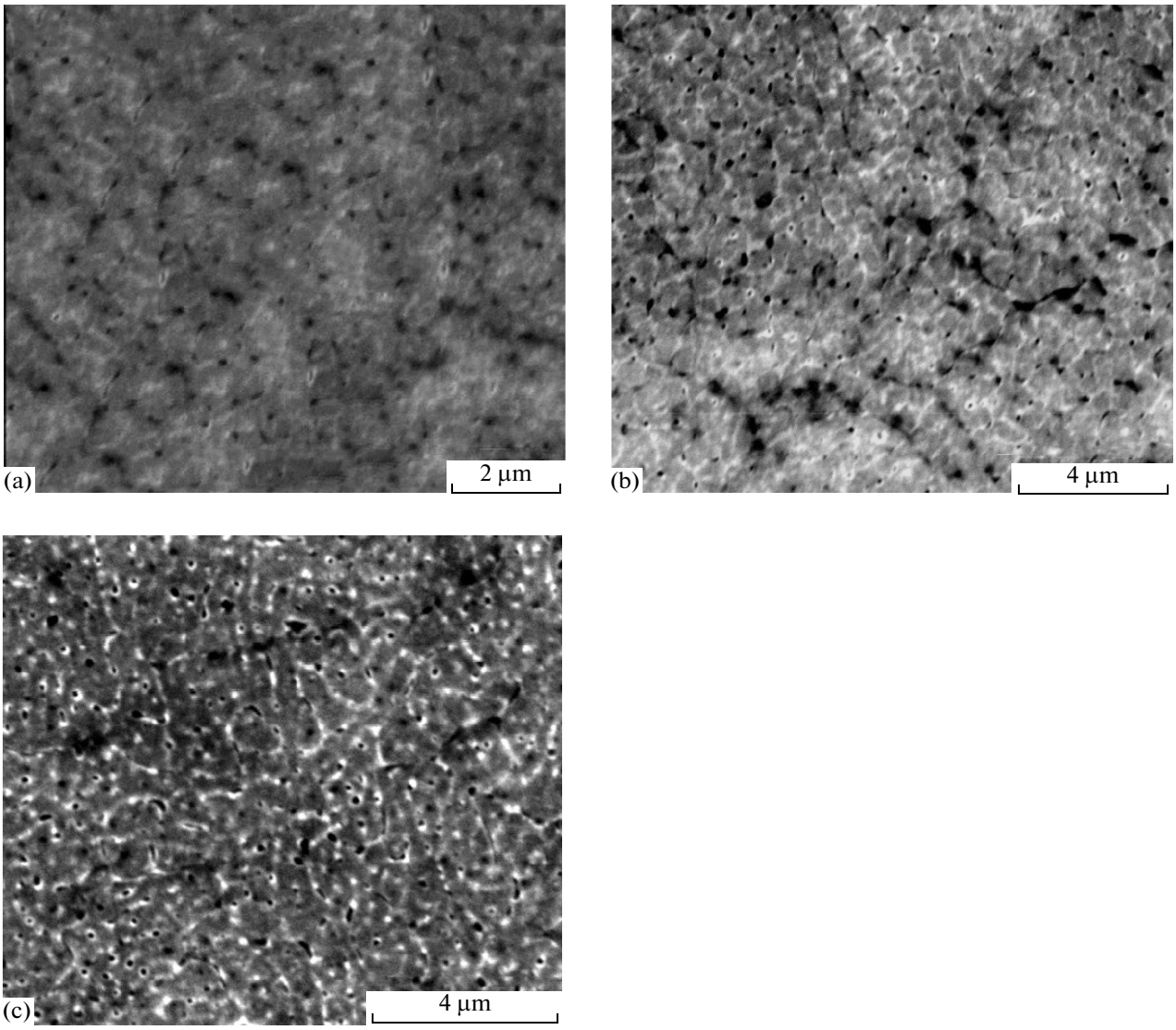

Fig. 1. Typical electron- microscopic images of (a) original RQM alloy, as well as of this alloy after annealing at (b) 550°C for 5 h and (c) 600°C for 2 h. SEM is secondary electron mode.

1 μm in size, prevail in the microstructure; they have a fairly uniform size distribution. Marked grain-boundary contrast can also be seen (both brighter continuous (along grain boundaries) and darker discrete, Figs. 1a–1c). Both modes of contrast become more intense when proceeding from Fig. 1a to Fig. 1c. This allows us to conclude that, on the one hand, this contrast mainly results from heat treatment and, therefore, from a possible process of the decomposition of the highly nonequilibrium solid solution of the alloy formed during RQM. On the other hand, when considering the origin of contrast in the SEM images, we should allow for the fact that, with a marked localization of some chemical elements, the smaller the atomic number Z of the segregated chemical element, the brighter the contrast; on the contrary, the larger the atomic numbers Z of the elements localized in the considered region, the darker the contrast, i.e., the greater the electron absorption.

The chemical composition of the alloy was determined by performing energy dispersive X-ray spectroscopy (EDS) analysis in local volumes a few tenths of a micron in size. It has been found that the distribution of the chemical elements over the volume of the alloy differs somewhat from the nominal composition (16.67 at % for each element) (Table 1). With allowance for our SEM and TEM data obtained by the EDS method with various sizes of the analytical electron probe and, therefore, the examined volume, it can be concluded that, in the cast RQM alloy, during the formation of SMC grains with typical equiaxed morphology, the intergrain joints have apparently become enriched in some chemical elements. Most likely, these elements form clusters (concentration fluctua-

Table 1. Elemental composition of original RQM equiatomic AlCrFeCoNiCu alloy as-determined by SEM and TEM EDS method

Chemical element	SEM		TEM	
	wt %	at %	wt %	at %
Al	7	14	6	13
Cr	15	15	16	16
Fe	19	18	18	17
Co	20	18	20	18
Ni	18	17	18	17
Cu	21	18	22	19
Total	100	100	100	100

Table 2. Elemental and phase compositions of the RQM equiatomic alloy after heating to 550°C and 2-h holding at the temperature, as-determined by TEM EDS

Chemical element	Matrix		B2–Cu–Ni–Co–Al	
	wt %	at %	wt %	at %
Al	7	13	5	10
Cr	14	15	10	11
Fe	20	20	12	12
Co	22	20	13	12
Ni	19	17	14	14
Cu	18	15	46	41
Total	100	100	100	100

tions and segregates). The phase separation of the alloy apparently occurs later during subsequent annealing (Fig. 1). Based on the SEM data, a conclusion can be drawn on the predominant localization of both lightest elements (apparently, Al) and heaviest elements (Cu, etc.) in the vicinity of grain boundaries.

Figure 2 shows typical TEM images of the original RQM alloy. In accordance with the images presented in Fig. 1, the SMC grain structure shown in Fig. 2a has distinct convex–concave boundaries with a pronounced contrast typical of heterogeneous phase separation. The images of some grains show ripple- or tweedlike contrast, which intensifies or extinguishes depending on the diffraction conditions, which can be varied by inclining the specimen in the goniometer (Fig. 2a–2d). According to the data of the identification of selected-area electron diffraction (SAED) patterns (the insets in Fig. 2), the alloy has a *B*2-type structure. The dark-field images taken in the *B*2-phase reflections (fundamental (Fig. 2d) and superlattice (Fig. 2c)) show the nonuniformly atomically ordered and, apparently, chemically inhomogeneous nanodomain substructure with an average size of separate domains equal to a few nanometers. This is additionally confirmed by the presence of tweed contrast of deformation origin in the bright-field image (Fig. 2b) and in the dark-field image in the fundamental reflection of the 110_{B2} type (Fig. 2d). The tweed contrast is also indicative of the coherent nature of the joining of nanodomains along antiphase domain boundaries.

Some information on the type of dominant short-wave and long-wave atomic displacements and coherent deformations can also be obtained from diffuse-scattering streaks that pass through the nonzero reflection in the SAED patterns along ⟨110⟩* directions. The satellites of the types 1/8–1/10 ⟨110⟩* show the presence of a modulated nanodomain substructure with a period of ~2 nm in the RQM alloy (see insets in Figs. 2b and 2c).

An SMC grain structure in the RQM alloy is retained after its annealing at 550 and 600°C (Figs. 3–5). The corresponding SAED patterns are given in the insets in Figs. 3 and 4. Their analysis shows that the *B*2-type atomic ordering and nanodomain modulation (with a somewhat higher, approximately twofold, period) are retained in the alloy. The diffraction contrast in the electron micrographs remains nonuniform over the grain volume. The elements of the contrast from nanoparticles are equiaxed in the RQM alloy annealed at 550°C for 2 h (Fig. 3) and gradually transform into the elements of contrast of Widmannstätten type oriented along the $\{110\}_{B2}$ planes after annealing at 550°C for 5 h and at 600°C for 2 h (Figs. 4 and 5). The pattern in the form of fragmented striated contrast is especially strongly pronounced in the images of the RQM alloy annealed at 600°C for 2 h (Fig. 5). In this case, the substructure of the alloy is apparently most close to the structure of the as-cast alloy [19]. The majority of precipitating particles, both globular and lamellar, are no more than 20–30 nm in size after annealing at 550°C; the lamellar particles are 200–300 nm long after annealing at 600°C for 2 h.

A number of diffuse effects are always observed in the SAED patterns of the annealed alloy identified in terms of the bcc *B*2-type structure with a lattice parameter a_{bcc} close to 0.288 nm. The SAED patterns that correspond to the cubic sections of the reciprocal lattice (zone axis $\langle 100\rangle_{bcc}$) contain also diffuse-scattering streaks passing through the nonzero reflection along ⟨110⟩* directions along which tetrads of equidistant first-type satellites are located, in the case of the original RQM alloy (see a typical example in Fig. 4). In the SAED patterns with the zone axis $\langle 110\rangle_{bcc}$, second-type diffuse satellites, i.e., 1/3 ⟨112⟩*, 1/3 ⟨111⟩*, 4/3 ⟨111⟩*, are often observed. As was noted above, we identify the appearance of the $1/n$ ⟨110⟩* satellites with the development of a nanodomain modulated substructure; the second-type satellites can result from the structural instability of ω-like displacements in the bcc phase [20] or in the other Ni_2Al metastable phase frequently observed in *B*2 Ni–Al alloys [21, 22].

Tables 2–4 present the data on the chemical composition of particles of various phases obtained by

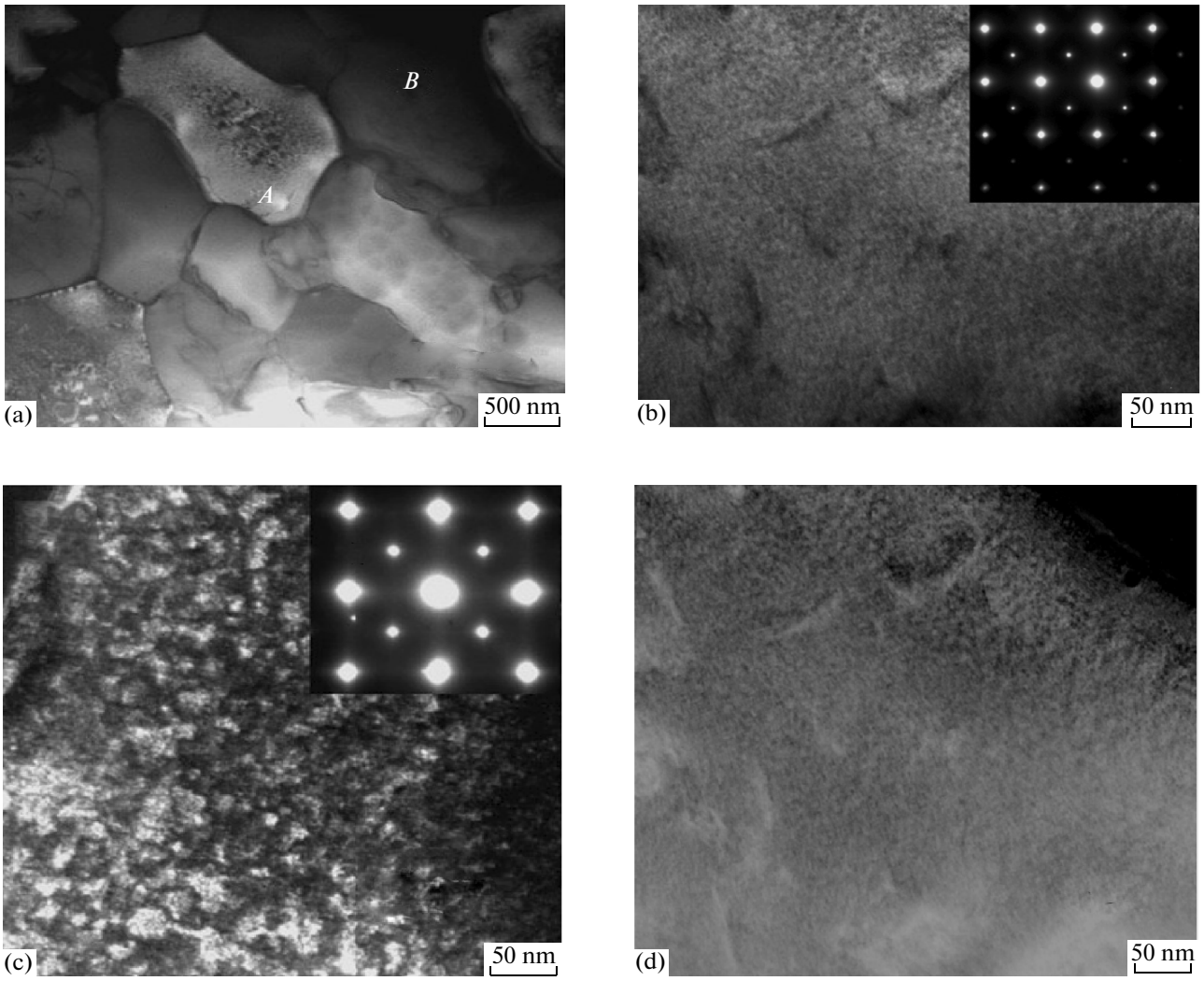

Fig. 2. Typical TEM images of the RQM AlCrFeCoNiCu alloy and selected-area electron-diffraction patterns (insets) corresponding to the zone axis (ZA) $[001]_{B2}$ of reflecting planes: (a, b) bright-field images and (c, d) dark-field images ((c) region *A* in the 100_{B2} reflection; and (b, d) region *B* in the 110_{B2} reflection).

TEM using EDS with a probing locality ~10 nm in the lateral section. The error of concentration measurement in these experiments was no less than 2–3%; therefore, we rounded the data to integer percentage values. When considering the results, we primarily note that different phase and chemical compositions were found in the RQM alloy after various heat treatments. After annealing at 550°C for 2 h, a matrix somewhat enriched in Fe, Cr, and Ni is identified along with the *B*2 phase in the form of equiaxed 10–20 nm nanoparticles based on the Cu–Ni–Co–Al multicomponent solid solution enriched in copper to 40 at % (Table 2). After annealing at 550°C for 5 h, there is also present a matrix somewhat enriched in Fe, Cr, and Ni and the particles of two nanophases are identified including, first, a *B*2 phase based on the Cu–Ni–Co–Al multicomponent solid solution enriched in copper to 40 at % and, second, apparently, a disordered *A*2 phase [19], which represents a solid solution enriched in Cr, Fe, and Co and depleted of Ni, Al, and Cu (Table 3). Finally, after annealing at 600°C for 2 h, the following three phases are identified in the alloy: first, a lamellar *B*2 phase based on the Cu–Ni–Al solid solution enriched in copper to 75 at %; second, apparently, an *A*2 phase that has a brighter contrast, the solid solution of which is even more enriched in Cr (up to 35 at %), Fe (up to 30 at %), and Co (up to 22 at %), but is noticeably depleted of Ni, Al, and Cu; and, third, a nanophase with 20–30-nm equiaxed particles based on a *B*2 Ni–Al–Co–Fe phase, whose solid solution also contains Cu and Cr (Table 4). Since it is difficult to exclude the possibility of the presence of other precipitating phases and the matrix substance itself, just in addition to the nanoparticles being examined, just in the zone of probing of the elemental composition, this may distort the quantitative data on their chemical composition.

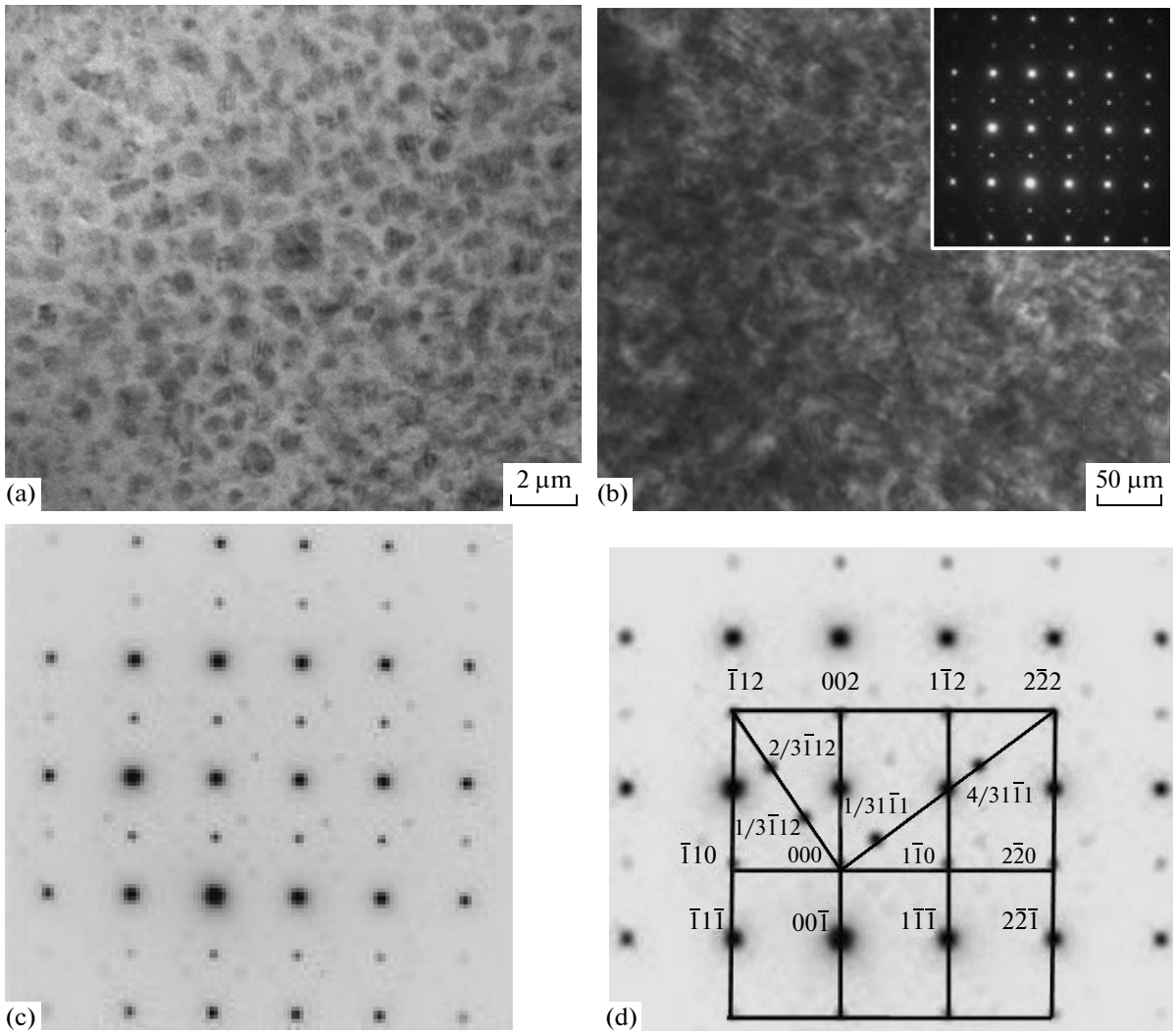

Fig. 3. Typical TEM images of the RQM AlCrFeCoNiCu alloy after annealing at 550°C for 2 h: (a) bright-field image and (b) dark-field image in 110_{B2} reflection; (c) and the inset in (b) corresponding SAED patterns (ZA $[110]_{B2}$); and (d) key pattern.

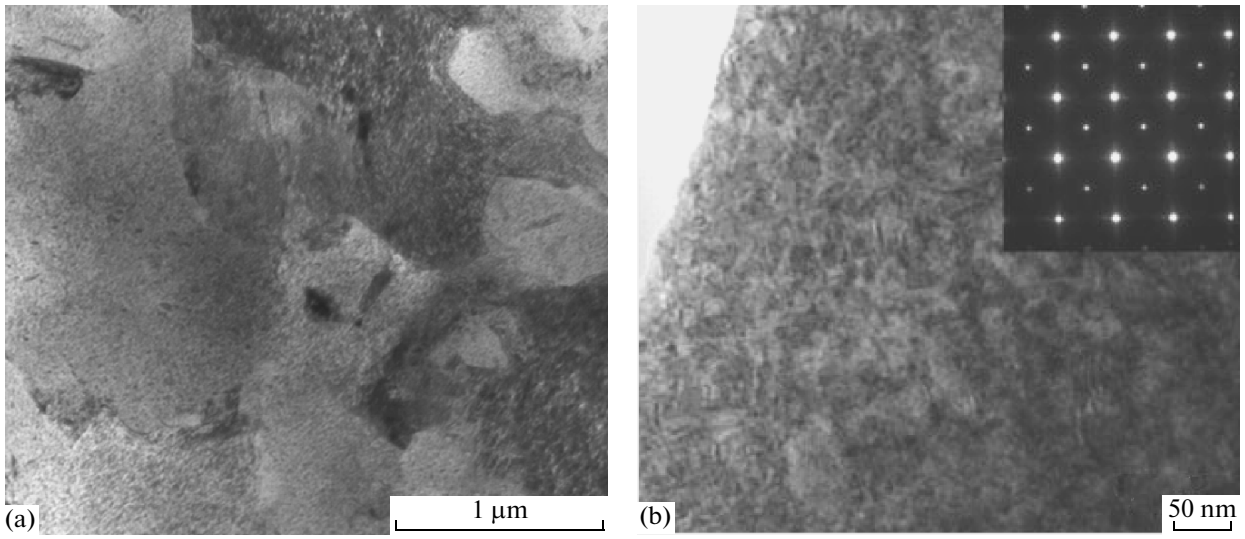

Fig. 4. Typical TEM images of theRQM AlCrFeCoNiCu alloy after annealing at 550°C for 5 h and the SAED pattern (inset, ZA $[001]_{B2}$).

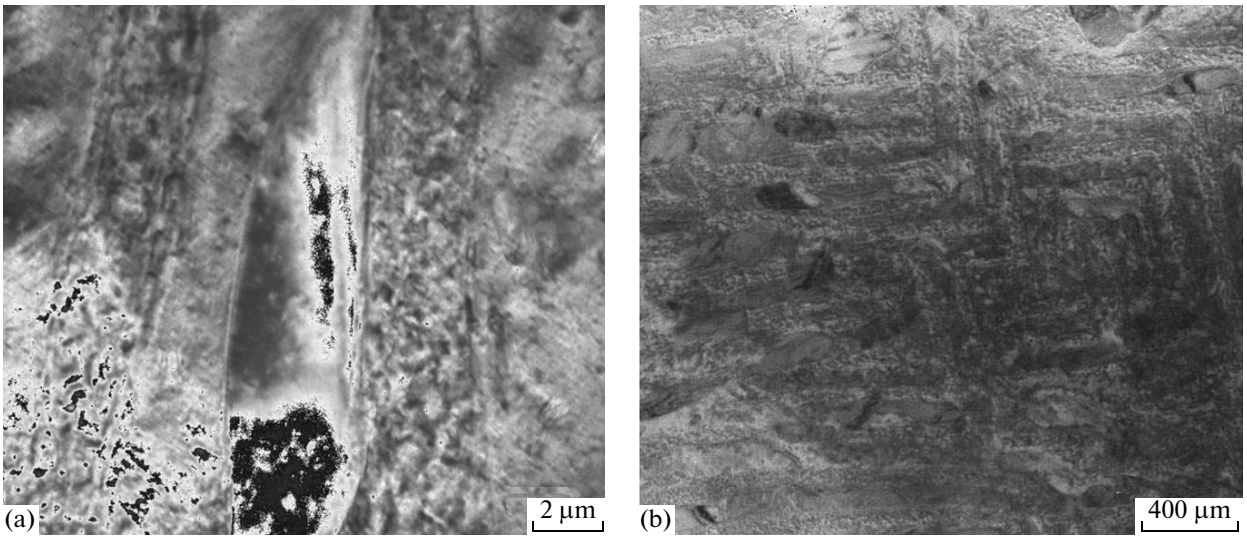

Fig. 5. Typical TEM images of theRQM AlCrFeCoNiCu alloy after annealing at 600°C for 2 h: (a) bright-field image and (b) dark-field image in the 110_{B2} reflection.

Figures 6 and 7, along with Table 5, present values of the elastic moduli, nano hardness, and total creep, as well as their dependences on the duration of annealing at 550°C. For comparison, the properties of the as-cast prototype alloy are also given in Table 5; the comparison shows that the elastic modulus of the as-cast alloy is substantially higher than that of the RQM alloy. This result is not unexpected, since the microstructure and the phase composition of the as-cast alloy after decomposition is in a more equilibrium multiphase state, which yields higher hardness, strength, and elastic characteristics. However, the annealing of the RQM alloy leads to a significant increase in the elastic modulus and, especially, hardness, which is now already 1.5–2 times higher than those of the as-cast or RQM alloy. In this case, the creep of the alloy has decreased substantially, which correlates with and is caused by the alloy strengthening (Fig. 7).

Finally, Fig. 8 shows the dependence of the electrical resistivity of the RQM alloy on cyclic temperature variations from room temperature (RT) to 300, 400, 500, and 650°C with intermediate measurements carried out upon cooling down to RT. An analysis of this dependence shows periodic changes in the electrical resistivity during the heating–cooling thermocycles and a gradual decrease in the electrical resistivity, which occurs as the alloy structure transforms into a more equilibrium state.

DISCUSSION

The polymetallic equiatomic AlCrFeCoNiCu alloy studied in this work belongs to high-entropy alloys. A specific feature of these alloys is the formation of phases on the basis of multicomponent solid solutions containing several (four, five, or more) alloying elements in nearly equiatomic concentrations [14]. It is

Table 3. Elemental and phase compositions of the RQM equiatomic alloy after heating to 550°C and 5-h holding at the temperature, as-determined by TEM EDS

Chemical element	Matrix		*B*2–Cu–Ni–Co–Al		*A*2–Cr–Fe–Co	
	wt %	at %	wt %	at %	wt %	at %
Al	8	16	6	12	7	13
Cr	16	16	9	10	25	25
Fe	20	19	12	12	23	21
Co	21	18	12	12	22	20
Ni	18	16	14	13	15	14
Cu	17	15	47	41	8	7
Total	100	100	100	100	100	100

Table 4. Elemental and phase compositions of the RQM equiatomic alloy after heating to 600°C and 2-h holding at the tempereture, as-determined by TEM EDS

Chemical element	*B*2–Cu–Ni–Al		*A*2–Cr–Fe–Co		*B*2–Ni–Al–Co–Fe	
	wt %	at %	wt %	at %	wt %	at %
Al	6	12	2	4	14	26
Cr	1	1	33	35	4	3
Fe	2	2	31	30	14	12
Co	2	2	24	22	21	19
Ni	8	8	7	7	35	30
Cu	81	75	3	2	12	10
Total	100	100	100	100	100	100

Table 5. Hardness and elastic modulus of as-cast and RQM alloys determined by the nanoindentation method under a load of 300 mN

Characteristics	Alloy state			
	as-cast	RQM	550°C, 0.5 h	550°C, 2 h
Hardness H_V, MPa	530	450	800	810
Elastic modulus E, GPa	180	40	95	115

expected that they should have simple disordered bcc or fcc structures with a random distribution of atoms and have to ensure substantial precipitation hardening and the thermal stability of their microstructure and properties even at elevated temperatures; they should also yield a number of some other attractive physicomechanical, chemical, and performance characteristics [14]. From the viewpoint of thermodynamics, the entropy of mixing is a crucial factor that is responsible for the formation of these polymetallic alloys based on multicomponent cubic solid solutions [14]. It is deemed that a noticeable rise in the entropy with an increasing number of components of equiatomic solid-solution alloys is accompanied by a corresponding decrease in the free energy (Gibbs energy) of this system, which stabilizes a nonequilibrium solid-solution state and makes it competitive with softening processes of structural and phase transformations that occur in the alloy [14].

When discussing the experimental results in the context of the above-said, it is important to note that a highly nonequilibrium, but inhomogeneous structural and phase state is retained, even in the as-cast high-entropy alloy slowly cooled at a rate of 10 K/s [19]. As was mentioned above, when studying the as-cast alloy of this composition [19], it was found that phase sepa-

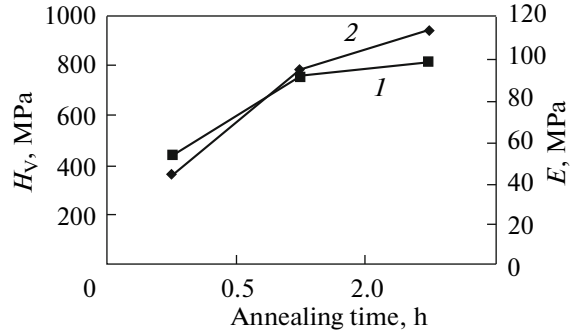

Fig. 6. Dependences of (*1*) the hardness and (*2*) the elastic modulus of the RQM alloy on the duration of annealing at 550°C recorded under a load of 300 mN.

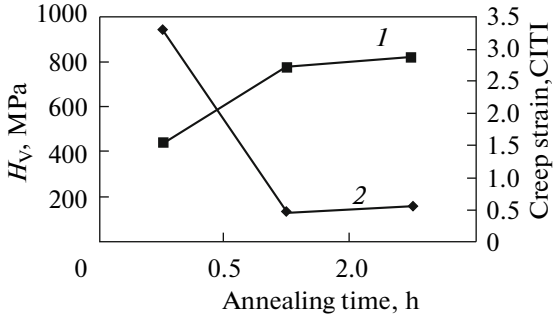

Fig. 7. Dependences of (*1*) the hardness H_V and (*2*) creep (in CITI units) of the RQM alloy on the duration of annealing at 550°C recorded under a load of 300 mN.

ration occurred in the initially arising bcc dendritic and fcc interdendritic structures during solidification and subsequent cooling at a rate of 10 K/s. This separation has led to the precipitation of six cubic phases (of the $A2$, $B2$, and $L1_2$ types) with various compositions and morphologies. The main specific features of these phases are a nanoscaled structure, a multicomponent chemical composition, as well as the pronounced periodic modulation with an alternation of phases and, therefore, of the chemical composition over the alloy volume. The cubic phases enriched in Cu–Ni–Al or based on Ni–Al–Co are atomically ordered, while the phase based on Cr–Fe–Co is atomically disordered.

In this work, for the first time, we carried out a systematic study of structural and phase transformations that occur in this high-entropy equiatomic AlCrFeCoNiCu alloy during ultrarapid quenching from the melt and subsequent heat treatments. The high cooling rate (~10^6 K/s) during the formation of thin lamellae of the RQM alloy should, to a great extent, naturally prevent it from possible separation and hinder the appearance of structures and phases typical of equilibrium states.

It has been found that an ultrafine-grained (SMC) structure is formed in the alloy during RQM and no dendrites are present in it. Long-range order was already detected in the original RQM alloy using, primarily electron microdiffraction (Fig. 2). Weak superlattice reflections, such as 100_{B2}, were also found by X-ray diffraction analysis. According to the TEM data, a nanodomain $B2$ structure has been formed in the RQM alloy and, in our opinion, the initial stage of the separation of the alloy has occurred, possibly, by the mechanism of heterogeneous decomposition at antiphase domain boundaries (APBs). However, this has not been confirmed by local elemental analysis carried out along APBs using EDS analysis because of the insufficient resolution of this method. In addition, we note that the results of selective chemical etching and specific features of contrast in the SEM and TEM images allow us to draw the conclusion on the heterogeneous enrichment of grain boundaries in chemical elements with primarily the lowest and the highest atomic numbers. The localization of these elements along the boundaries is clearly different. Judging from continuous brighter fringes of contrast along grain boundaries, the lighter chemical elements (primarily aluminum) form continuous near-boundary layers. Heavier metals, most likely copper, are located along the boundaries as discrete regions and can be seen in the form of dark spots of contrast in white-imaged envelopments (Fig. 1).

All of the above-mentioned specific features of the structural and phase state of the RQM alloy exhibit noticeable evolution during annealing at 550 and 600°C (Fig. 9). Their main signs are as follows:

—the gradual formation of a small amount of crystalline multicomponent phases that are fairly uniformly distributed over the alloy volume: initially, at 550°C, the first phase enriched in copper appears; then, a second phase is formed that is enriched in Cr, Fe, and Co, in which the first phase is mainly depleted; and, finally, at 600°C, the formation of a third phase based on the Ni–Al–Co system and the disappearance of the matrix, the chemical composition of which would be close to the initial composition;

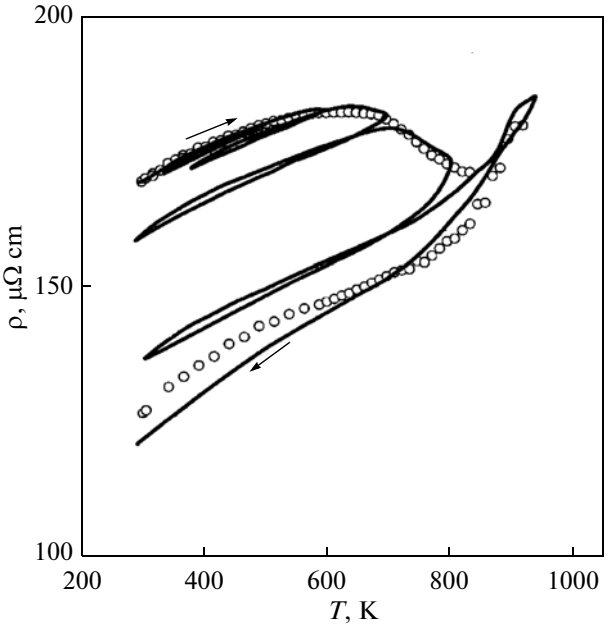

Fig. 8. Temperature dependence of the electrical resistivity $\rho(T)$ of RQM alloy during cyclic temperature variations RT → 300°C → RT → 400°C → RT → 500°C → RT → 650°C at a heating/cooling rate of ~2 K/min.

—the presence of simple cubic phases, both atomically ordered ($B2$ type) and disordered ($A2$);

—the nanosized scale of the phases and the prevalence of isotropic (equiaxed) or medium-anisotropic (cuboidal-lamellar) morphologic forms due to the uniformly discrete spatial ordering of all nanophases;

—the nanomodulated character of the distribution of the chemical composition and of the nanophases (and, as is supposed in some works, the spinodal mechanism of the decomposition of the solid-solution phases, which is especially close to the RQM state);

—the implementation of rational size and orientation relationships between the phases and, apparently, a predominantly coherent character of their interphase joints, which follows primarily from the data of electron microscopy.

In conclusion, returning to the initial formulation of the problem [14], we note that, despite predictions and the use of ultrarapid melt quenching to synthesize this high-entropy alloy, neither amorphous nor even the nanocrystalline structural state, i.e., partially or fully atomically disordered, with a random distribu-

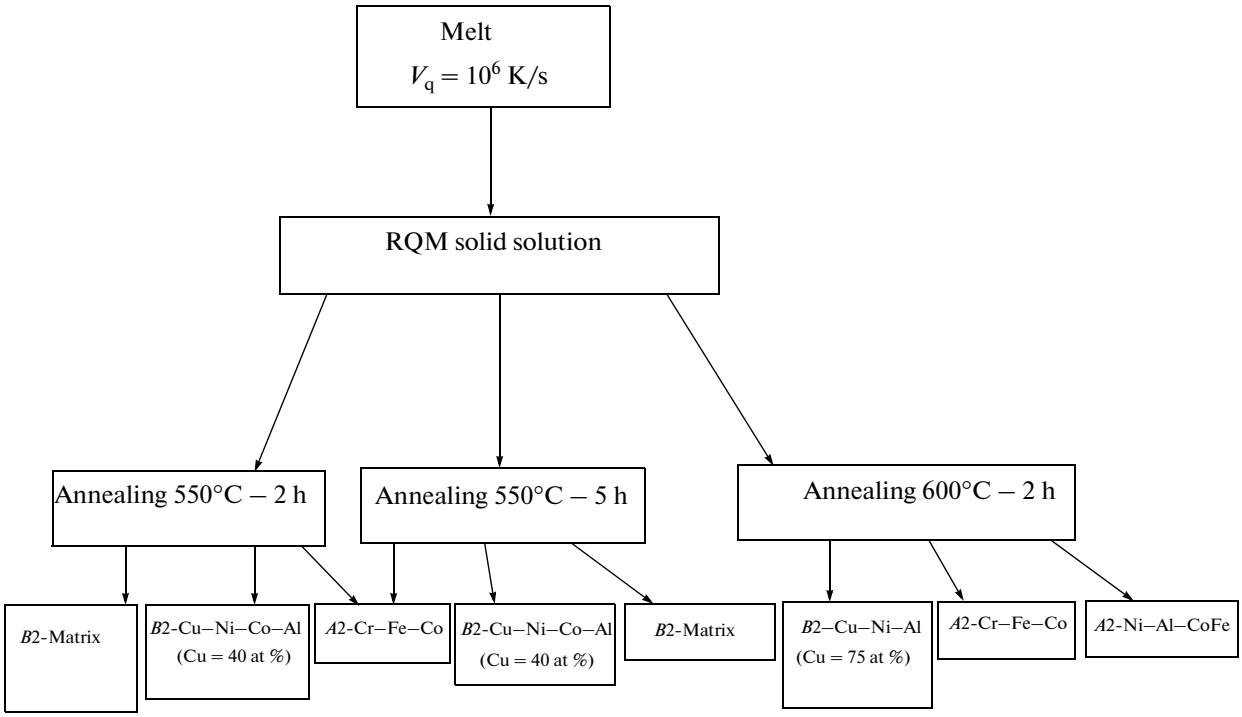

Fig. 9. Diagram of phase separation in RQM AlCrFeCoNiCu alloy.

tion of chemical elements over lattice sites, has been achieved in this alloy, unlike a number of common low-entropy medium-alloy intermetallic alloys [23, 24]. On the contrary, after RQM, the alloy is practically atomically ordered and has a submicrocrystalline grain structure, although it is multinanodomain and nanophase.

CONCLUSIONS

Based on the study of structural and phase transformations in the multicomponent high-entropy equiatomic AlCrFeCoNiCu alloy synthesized by rapid quenching from the melt using the splat-quenching method, the following conclusions can be drawn:

(1) During solidification under conditions of ultrarapid cooling ($V_q \approx 10^6$ K/s), a homogeneous ultrafine-grained submicrocrystalline bcc structure has been formed; no dendrites or phases of other structure types have appeared.

(2) The basic structural and phase state of the alloy after quenching is characterized by a nanodomain bcc (*B*2 type) superstructure modulated with a period of ~2 nm that may possibly appear along antiphase domain boundaries at the initial stage of atomic phase separation. The observed signs of contrast in electron-microscopic images allow us to conclude that the heterogeneous enrichment of the grain boundaries takes place in some chemical elements, which form continuous and discrete concentration segregates or precipitates of isostructural nanophases. The experimentally determined chemical composition, i.e., the average composition with a lateral locality of ~10 nm, is almost the same as the nominal alloy composition.

(3) The phases that precipitate during annealing at 550 and 600°C are characterized by a nanoscale and have a bcc mainly equiaxed atomically ordered (*B*2-type) or disordered (*A*2-type) structures. As the duration of annealing at 550°C increases to 5 h or the annealing temperature increases to 600°C (for 2 h), the structural elements also take a cuboidal-lamellar shape. These precipitated phases are uniformly distributed relative to one another and over the alloy volume, have a size-orientational and coherent bonding with the matrix and between themselves, which also follows from an analysis of selected-area electron-diffraction patterns.

(4) All nanophases are multicomponent solid solutions based on Cu–Ni–Co–Al, Cr–Fe–Co, and Ni–Al–Co–Fe systems and are enriched in several elements, which is accompanied by the pronounced nanomodulation of the elemental and phase compositions over the alloy volume. This is well confirmed by the data obtained for this alloy by transmission electron microscopy, SAED patterns, and energy dispersive X-ray spectroscopy.

(5) Annealing at 550°C leads to a substantial (by a factor of 1.5–2) increase in the elastic modulus and, especially, hardness, which is accompanied by a considerable (7-fold) decrease in the creep of the RQM alloy.

ACKNOWLEDGMENTS

The work was supported in part by budget projects of the Presidium of the Russian Academy of Sciences (no. 12-I-2-2031) and the Ural Branch of the Russian Academy of Sciences (no. 12-M-235-2063).

REFERENCES

1. M. L. Bernshtein, *Thermomechanical Treatment of Alloys* (Metallurgiya, Moscow, 1972), in 2 vols. [in Russian].
2. B. A. Kolachev, V. A. Livanov, and V. I. Elagin, *Metal Science and Thermal Treatment of Non-Ferrous Metals and Alloys* (Metallurgiya, Moscow, 1972) [in Russian].
3. G. V. Kurdjumov, L. M. Utevskii, and R. I. Entin, *Transformations in Iron and Steel* (Nauka, Moscow, 1977) [in Russian].
4. I. I. Fridlyander, *Aluminum Deformable Structural Alloys* (Metallurgiya, Moscow, 1979) [in Russian].
5. A. M. Glezer and V. V. Molotilov, *Ordering and Deformation of Iron Alloys* (Metallurgiya, Moscow, 1984) [in Russian].
6. V. N. Khachin, V. G. Pushin, and V. V. Kondrat'ev, *Titanium Nickelide: Structure and Properties* (Nauka, Moscow, 1992) [in Russian].
7. V. G. Pushin, V. V. Kondrat'ev, and V. N. Khachin, *Pretransition Phenomena and Martensite Transformations* (Ural. Otd. Ross. Akad. Nauk, Ekaterinburg, 1998) [in Russian].
8. E. N. Kablov and E. R. Golubovskii, *Heat Resistance of Nickel Alloys* (Mashinostroenie, Moscow, 1998) [in Russian].
9. "To 70th anniversary of VIAM: A special issue," Metal Sci. Heat Treat., No. 7 (2002).
10. B. A. Greenberg and M. A. Ivanov, *Ni_3Al and TiAl Intermetallic Componds: Microstructure and Deformation Behavior* (Ural. Otd. Ross. Akad. Nauk, Ekaterinburg, 2002) [in Russian].
11. V. G. Pushin, S. D. Prokoshkin, R. Z. Valiev, V. Brailovskii, E. Z. Valiev, A. E. Volkov, A. M. Glezer, S. V. Dobatrin, E. F. Dudarev, V. T. Zhu, Yu. G. Zainulin, Yu. R. Kolobov, V.V. Kondratiev, A. V. Korolev, A. I. Korshunov, N. I. Kourov, N. V. Kudrevatykh, A. I. Lotkov, L. L. Meisner, A. A. Popov, N. N. Popov, A. I. Razov, M. A. Khusainov, Yu. I. Chumlyakov, S. V. Andreev, A. A. Baturin, S. P. Belyaev, V. N. Grishkov, D. V. Gunderov, A. P. Dyupin, K. V. Ivanov, V. I. Itin, M. K. Kasymov, O. A. Kashin, I. V. Kireeva, A. I. Kozlov, T. E. Kuntsevich, N. N. Kuranova, N. Yu. Pushina, E. P. Ryklina, A. N. Uksusnikov, I. Yu. Khmelevskaya, A. V. Shelyakov, V. Ya. Shklover, E. V. Shorokhov, and L. I. Yurchenko, *Titanium Nickelide Alloys with Shape Memory. Ch. I: Structure, Phase Transformations and Properties* (Ural. Otd. Ross. Akad. Nauk, Ekaterinburg, 2006) [in Russian].
12. V. G. Pushin, "Alloys with a Thermomechanical Memory: Structure, Properties, and Application," Phys. Met. Metallogr. **90** (Suppl. 1), S68–S95 (2000).
13. V. Brailovski, I. Yu. Khmelevskaya, S. D. Prokoshkin, V. G. Pushin, E. P. Ryklina, and R. Z. Valiev, "Foundations of heat and thermomechanical treatments and their effect on the structure and properties of titanium nickelide–based alloys," Phys. Met. Metallogr. **97** (Suppl. 1), S3–S55 (2004).
14. J. W. Yeh, Y. L. Chen, S. J. Lin, and S. K. Chen, "High-Entropy Alloys—A New Era of Exploitation," Mat. Sci. Forum **560**, 1–9 (2007).
15. C. J. Tong, Y. L. Chen, S. K. Chen, J. W. Yeh, T. T. Shun, C. H. Tsau, S. J. Lin, and S. Y. Chang, "Microstructure characterization of Al_xCoCrCuFeNi high-entropy alloy system with multiprincipal elements," Met. Mater. Trans. A **36**, 881–893 (2005).
16. C. C. Tung, J. W. Yeh, T. T. Shun, S. K. Chen, Y. S. Huang, and H. C. Chen, "On the elemental effect of AlCoArCuFeNi high-entropy alloy system," Mater. Lett. **61**, 1–5 (2007).
17. X. F. Wang, Y. Zhang, Y. Qiao, and G. L. Chen, "Novel microstructure and properties of multicomponent CoCrCuFeNiTi$_x$ alloys," Intermetallics **15**, 357–362 (2007).
18. S. Singh, N. Wanderka, B. S. Murty, U. Glatzel, and J. Banhart, "Decomposition in multi-component AlCoCrCuFeNi high-entropy alloy," Acta Mater. **59**, 182–190 (2011).
19. M. V. Ivchenko, V. G. Pushin, A. N. Uksusnikov, and N. Wanderka, "Microstructure features of high-entropy equiatomic cast AlCrFeCoNiCu Alloys," Phys. Met. Metallogr. **114**, 514–520 (2013).
20. V. V. Kondrat'ev and V. G. Pushin, "Premartensitic state in metals, their alloys and compounds: Experimental results, models, structures, classification," Fiz. Met. Metalloved. **60** (4), 629–650 (1985).
21. V. G. Pushin, S. P. Pavlova, and L. I. Yurchenko, "Study of pretransition states and martensite transformation in Ni–Al *B*2 alloys," Fiz. Met. Metalloved. **67** (1), 164–174 (1989).
22. V. G. Pushin, L. I. Yurchenko, A. Yu. Sokolova, and L. Yu. Ivanova, "Premartensitic phenomena in *B*2 Ni–Al alloys: An electron microscopic, X-ray, and electron diffraction study," Phys. Met. Metallogr. **78**, 657–665 (1994).
23. V. G. Pushin, S. B. Volkova, and N. M. Matveeva, "Structural and phase transformations in quasi-binary TiNi–TiCu alloys rapidly quenched from the melt: I. High-copper amorphous alloys," Phys. Met. Metallogr. **83**, 275–282 (1997).
24. T. E. Kuntsevich and V. G. Pushin, "The microstructure and properties of rapidly quenched Ti-rich Ti–Ni binary alloys with shape memory effects," Phys. Met. Metallogr. **105**, 56–63 (2008).

Translated by D. Tkachuk